PAPER

Optimizing surface residual alkali and enhancing electrochemical performance of $LiNi_{0.8}Co_{0.15}Al_{0.05}O_2$ cathode by LiH_2PO_4

View the article online for updates and enhancements.

Optimizing surface residual alkali and enhancing electrochemical performance of LiNi$_{0.8}$Co$_{0.15}$Al$_{0.05}$O$_2$ cathode by LiH$_2$PO$_4$

Wendong Cheng[1] , **Shuai Hao**[1], **Yuyao Ji**[1], **Lei Li**[1], **Ling Liu**[1,2], **Yu Xiao**[1], **Yuxuan Wu**[1], **Jinsheng Huo**[1], **Fan Tang**[3] and **Xingquan Liu**[1]

[1] School of Materials and Energy, University of Electronic Science and Technology of China, Chengdu 610054, People's Republic of China
[2] Sichuan Fuhua New Energy Hi-Tech Co., Ltd, Mianyang 621006, Sichuan, People's Republic of China
[3] School of Materials Science and Engineering, Hubei University, Hubei 430062, People's Republic of China

E-mail: Lxquan@uestc.edu.cn

Abstract

LiNi$_{0.8}$Co$_{0.15}$Al$_{0.05}$O$_2$ (NCA), a promising ternary cathode material of lithium-ion batteries, has widely attracted attention due to its high energy density and excellent cycling performance. However, the presence of residual alkali (LiOH and Li$_2$CO$_3$) on the surface will accelerate its reaction with HF from LiPF$_6$, resulting in structural degradation and reduced safety. In this work, we develop a new coating material, LiH$_2$PO$_4$, which can effectively optimize the residual alkali on the surface of NCA to remove H$_2$O and CO$_2$ and form a coating layer with excellent ion conductivity. Under this strategy, the coated sample NCA@0.02Li$_3$PO$_4$ (P2-NCA) provides a capacity of 147.8 mAh g^{-1} at a high rate of 5 C, which is higher than the original sample (126.5 mAh g^{-1}). Impressively, the cycling stabilities of P2-NCA under 0.5 C significantly improved from 85.2% and 81.9% of pristine-NCA cathode to 96.1% and 90.5% at 25 °C and 55 °C, respectively. These satisfied findings indicate that this surface modification method provides a feasible strategy toward improving the performance and applicability of nickel-rich cathode materials.

Keywords: LiNi$_{0.8}$Co$_{0.15}$Al$_{0.05}$O$_2$, LiH$_2$PO$_4$, residual alkali, coating layer, cycling stability
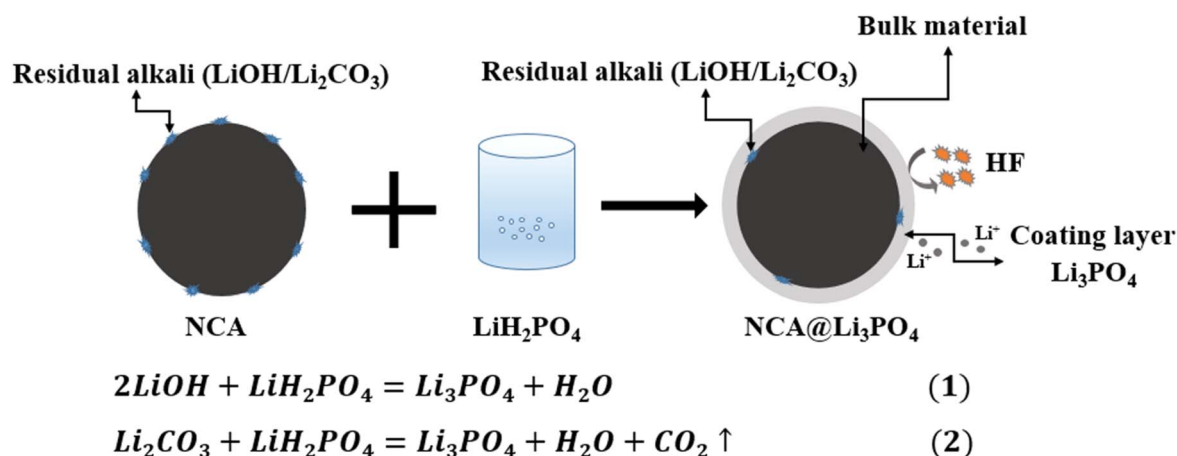
(Some figures may appear in colour only in the online journal)

1. Introduction

Nickel-rich LiNi$_{1-x}$M$_x$O$_2$ (M = Co, Mn, Al; $x<0.6$) layered materials are widely used in the field of high-power lithium batteries due to their low cost, high capacity, high reproducibility and facile preparation [1–3]. LiNi$_{0.8}$Co$_{0.15}$Al$_{0.05}$O$_2$ (NCA) is a promising candidate of the nickel-rich cathode materials due to its high reversible stability, excellent processability, and superior storage performance [4, 5]. However, to avoid lithium loss due to lithium volatilization during the sintering process, excessive lithium sources will be added during the synthesis process, resulting in excess residual alkali (LiOH and Li$_2$CO$_3$) on the surface of the final NCA particles [6]. Consequently, plethoric

residual alkali on the surface will react with the Lewis acid produced by the hydrolysis of the electrolyte to generate H$_2$O and CO$_2$, which will seriously affect the electrochemical performance and safety of the batteries [7]. In addition, the exposed NCA particles are susceptible to corrosion by Lewis acid, resulting in the dissolution of transition metal ions from the lattice into the electrolyte or even shuttle to the negative electrode, hence the lattice structure undergoes continuous degradation. As the side reaction continues, the reversible capacity gradually decreases and the cycle stability deteriorates [8].

In order to solve these problems, surface coating of NCA is a particularly effective strategy, which can block the direct contact between NCA and electrolyte, thereby reducing the side

Scheme 1. The mechanism diagram of LiH$_2$PO$_4$ modified NCA.

$$2LiOH + LiH_2PO_4 = Li_3PO_4 + H_2O \qquad (1)$$

$$Li_2CO_3 + LiH_2PO_4 = Li_3PO_4 + H_2O + CO_2 \uparrow \qquad (2)$$

reactions [9]. However, the traditional coating method rarely optimizes the residual alkali on the surface and the majority of the coating materials are Li-ion insulators with lower Li-ion diffusion coefficient, which hinders Li-ion transportation at the electrode interface and thus leads to the poor rate capability [10–12]. Considering these circumstances, we develop a new coating material, LiH$_2$PO$_4$, to modify the surface of NCA to enhance electrochemical performance, which has never been reported before. Notably, the LiH$_2$PO$_4$ can not only react with residual alkali on the surface to remove H$_2$O and CO$_2$, but also can form a coating layer with excellent ion conduction to enhance its surface ionic conductivity, as illustrated in scheme 1.

In this work, we successfully prepared LiH$_2$PO$_4$ modified NCA cathode material. On the one hand, this phosphate can avoid direct contact between NCA and electrolyte, thereby reducing the side reactions during the charging and dischar-ging process, and effectively alleviating the degradation of the secondary particle structure. On the other hand, such a layer can react with the residual alkali on the surface of the particles to form Li$_3$PO$_4$, a fast ion conductor, which can increase its dynamic performance. Under this strategy, the rate perfor-mance of NCA@0.02Li$_3$PO$_4$ (P2-NCA) significantly enhan-ces, which benefits from the formation of a fast ion conductor protective layer on the surface. It is noteworthy that due to removal of H$_2$O and CO$_2$, and the protective effect of the phosphate coating layer on the secondary particles, the cycle stability of the battery has also greatly improved.

2. Materials and methods

2.1. Chemicals

The Ni$_{0.8}$Co$_{0.15}$Al$_{0.05}$(OH)$_2$ precursor was purchased from Sichuan Fuhua New Energy Hi-Tech Co., Ltd Lithium dihydrogen phosphate (LiH$_2$PO$_4$) was purchased from Sigma-Aldrich Chemical Reagent Co., Ltd Lithium hydroxide (LiOH·H$_2$O) and ethanol (C$_2$H$_5$OH) were purchased from Chengdu Kelong Chemical Reagent Factory. The water used in all experiments was purified by the Millipore system. All
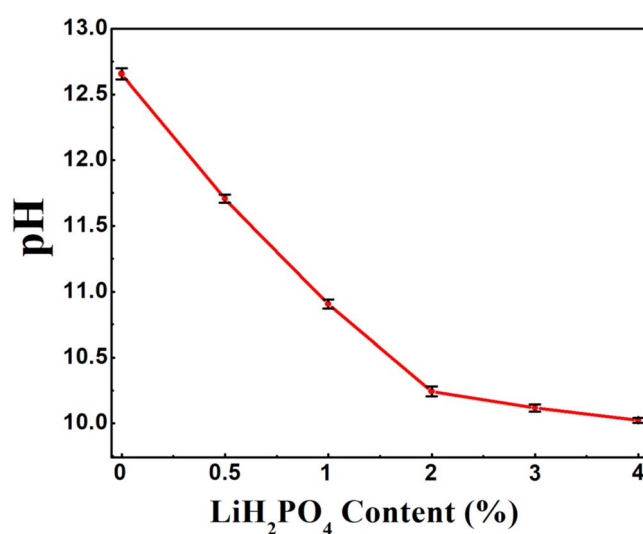
Figure 1. The pH values and error bars of samples with different LiH$_2$PO$_4$ content.

chemicals are used as received and no further purification is required.

2.2. Preparation of LiNi$_{0.8}$Co$_{0.15}$Al$_{0.05}$O$_2$ and LiNi$_{0.8}$Co$_{0.15}$Al$_{0.05}$O$_2$@xLi$_3$PO$_4$

In order to prepare LiNi$_{0.8}$Co$_{0.15}$Al$_{0.05}$O$_2$ (NCA) cathode materials, commercial Ni$_{0.8}$Co$_{0.15}$Al$_{0.05}$(OH)$_2$ precursor and LiOH·H$_2$O were added to 10 ml deionized water according to the molar ratio of 1:1.15 (mass ratio = 4.5570 g:2.4127 g) and fully stirred 30 min, then 10 ml absolute ethanol was added as a dispersant to make the two fully and uniformly mixed (repeat three times) until dry to obtain a green mixture. After drying at 105 °C for 24 h, the green mixture was pre-fired at 500 °C for 6 h and sintered at 720 °C for 15 h in a tube furnace under flowing oxygen to obtain the black powders, NCA. The synthesis method of NCA@Li$_3$PO$_4$ could be divided into two parts. First, according to the molar ratio of LiNi$_{0.8}$Co$_{0.15}$Al$_{0.05}$O$_2$: LiH$_2$PO$_4$ = 1:x (x = 0.005, 0.01, 0.02, 0.03, 0.04), LiH$_2$PO$_4$ was weighed and dispersed in 30
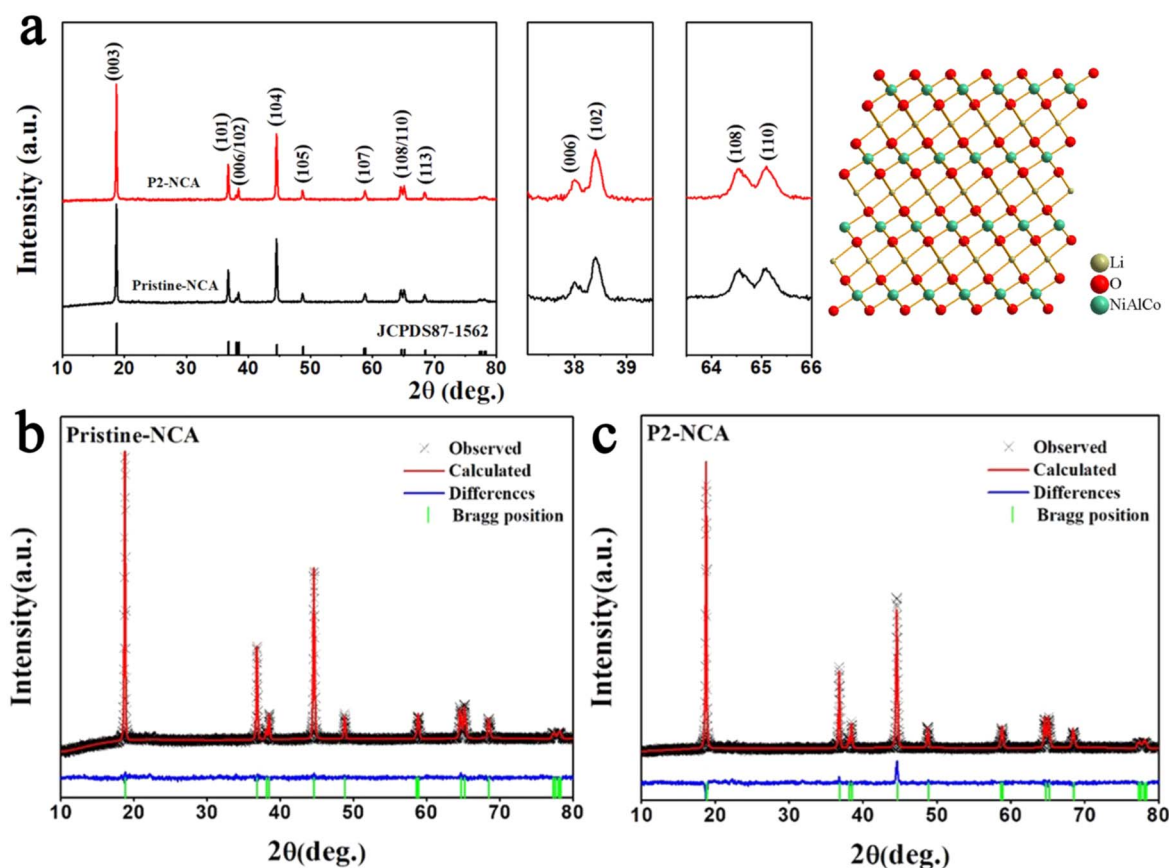
Figure 2. (a) XRD patterns of Pristine-NCA and P2-NCA, and the crystal structure model; Rietveld refinement results for the (b) Pristine-NCA, (c) P2-NCA samples.

Table 1. Rietveld refinement results for NCA, and P2-NCA samples.

Samples	a (Å)	c (Å)	V (Å^3)	Ni^{2+} in Li site (%)	R_p	R_{wp}
Pristine-NCA	2.8676	14.2023	100.95(4)	3.18	2.91	2.23
P2-NCA	2.8675	14.2028	100.96(1)	1.92	2.78	2.24

ml absolute ethanol, then ultrasonicated for 10 min to make it fully dispersed. Subsequently, the prepared NCA cathode materials (4.8042 g) were put into it and fully stirred until the ethanol was completely volatilized. Finally, after drying at 105 °C for 24 h, the obtained powders were annealed in a tube furnace at 550 °C under flowing oxygen for 8 h to obtain NCA@xLi$_3$PO$_4$ cathode material. For simplicity, the samples of NCA@xLi$_3$PO$_4$ (x = 0.005, 0.01, 0.02, 0.03, 0.04) were marked as P0.5-NCA, P1-NCA, P2-NCA, P3-NCA and P4-NCA, respectively.

2.3. Characterizations

The phase identification is analyzed by powder x-ray diffraction (XRD, Bruker D8 Advance, 2θ range: 10°–80°) with a step length of 0.02°, which uses Cu Kα radiation. Rietveld refinement is obtained through GSAS software. The morphological characteristics are obtained by performing field

emission scanning electron microscopy (SEM, ZEISS Gemini 300). The distribution of the elements is collected by mapping measurement with an energy dispersive spectrometer (EDS, OXFORD Xplore). The element types and valence states are obtained by x-ray photoelectron spectroscopy (XPS, Thermo Scientific K-Alpha, Al Kα radiation). The spectra were corrected with the standard C 1s spectrum (284.8 eV). The pH meter (PHS-3C) is used to detect the alkalinity of all samples. The structure and distribution of the surface cladding layer are observed by field emission transmission electron microscope (FETEM, FEI Tecnai G2 F20).

2.4. Electrochemical measurements

The electrochemical properties of all samples are measured using a typical CR2025 coin cell. The battery is assembled in a glove box (Mikrouna universal 2440) filled with argon atmosphere (O$_2$ and H$_2$O content < 0.1 ppm) in which the
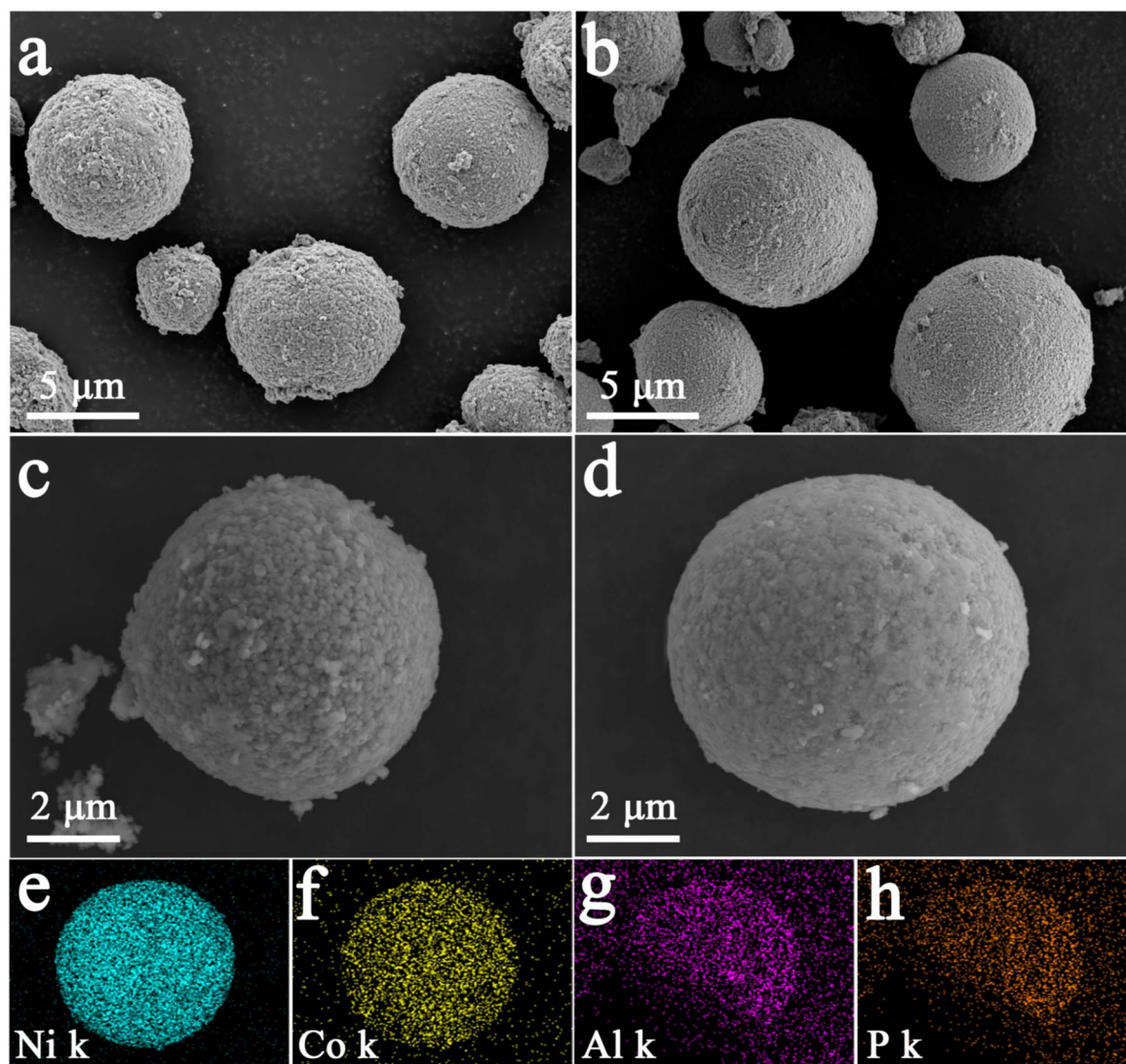
Figure 3. SEM images of (a) (c) Pristine-NCA and (b) (d) P2-NCA. EDS mapping of (c) Ni, (d) Co, (e) Al and (f) P of P2-NCA.

positive case, working electrode, separator Celgard 2400, lithium metal plate, gasket and negative case are assembled in sequence and electrolyte (mixture of 1M LiPF$_6$ and V_{EC}:V_{DEC} = 1:1) is fully infiltrated between the positive electrode and negative electrode. The working electrode is prepared by fully and uniformly mixing the active materials, acetylene black and PVDF (mass ratio 85:10:5) in NMP, and immediately coating on the current collector (aluminum foil) while keeping the mass load at 3–4 mg cm^{-2}. After drying in a vacuum drying oven at 105 °C to remove NMP, the aluminum foil was cut into discs with a diameter of 12 mm. A battery test system (LAND, China) was used to analyze the electrochemical performance of manufactured batteries under different current densities (2.75–4.3 V, 1 C = 200 mA g^{-1}). The cyclic voltammetry curve (CV, CHI-660E) was obtained at a scan rate of 0.1 mV s^{-1} and the electrochemical impedance spectroscopy (EIS, CHI-660E) was tested in the frequency range of 100 kHz to 0.01 Hz.

3. Results and discussion

Above all, in order to verify the optimization of LiH$_2$PO$_4$ on the residual alkali on the surface of NCA, we tested the pH of all samples. As shown in figure 1, Pristine-NCA demonstrates the highest pH value. With the increase of phosphate in the preparation process, the pH value shows a gradual decrease trend. Impressively, when the content LiH$_2$PO$_4$ exceeds 2%, pH value tends to decrease gradually gentle proved NCA surface residual alkali has been significantly optimized. Notably, the continuous decrease in the pH of P3-NCA and P4-NCA indicates that the LiH$_2$PO$_4$ mixed in the P0.5-NCA, P1-NCA and P2-NCA samples completely participate in the reaction with the surface alkali. According to previous research reports, the residual alkali on the surface is a critical factor leading to the degradation of the material structure during the cycle [5]. However, the addition of overmuch phosphate will form an overly thick coating layer, thereby
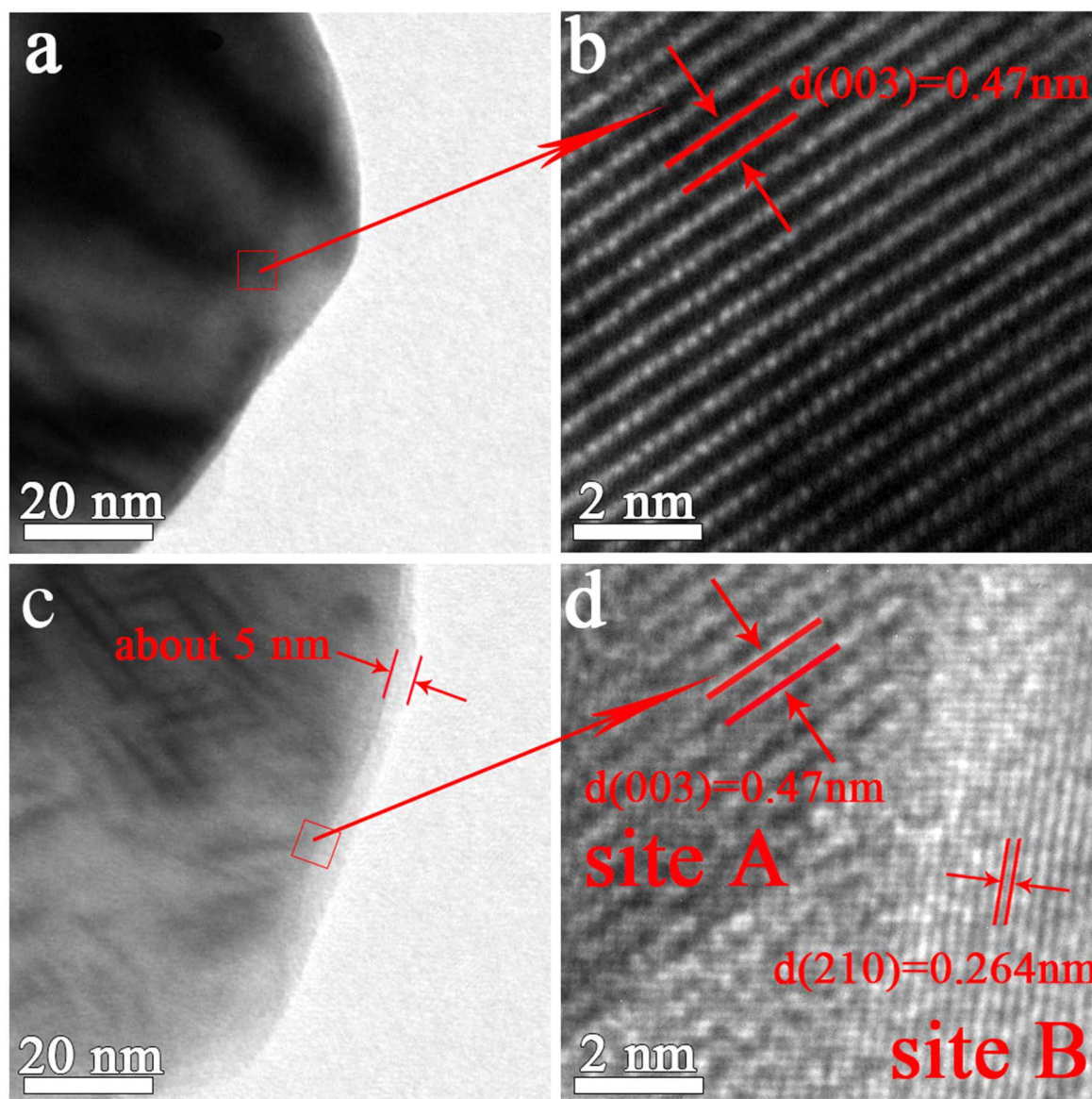
Figure 4. FETEM diagrams of (a) Pristine-NCA and (c) P2-NCA. High-resolution FETEM images of (b) Pristine-NCA and (d) P2-NCA.

hindering the dynamic performance of NCA. Therefore, 2% LiH2PO4 was selected as the optimal coating amount and a series of characterizations were performed on Pristine-NCA and P2-NCA.

Figure 2(a) shows the XRD patterns of Pristine-NCA and P2-NCA, and the crystal structure model. Compared with the standard PDF card (JCPDS 87-1562), it is found that both of them match the α-NaFeO$_2$ layered structure (the space group of R-3m) [13]. In addition, there are no evident differences in the crystal structure of Pristine-NCA and P2-NCA, and there is no diffraction peak related to the phosphate phase, which may be due to the low concentration of the phosphate coating layer [14]. More importantly, the obvious splitting of the (006)/(102) peak and (108)/(110) peak indicates their good crystallinity [15]. The results of Rietveld refinement and the obtained lattice parameters are shown in figures 2(b) and (c) and table 1, respectively. The error coefficients (R_p and R_{wp})

are far less than 10%, indicating the reliability of the refined results. The results show that P2-NCA has similar lattice parameters to Pristine-NCA, suggesting that the coating layer has little effect on the crystal structure of the host material [16]. It is worth noting that the decrease of the Li$^+$/Ni^{2+} mixing value proves the effective removal of residual alkali on the surface of the material [17].

The SEM images of Pristine-NCA (figures 3(a) and (c)) and P2-NCA (figures 3(b) and (d)) show that they have similar spherical and grain sizes (approximately 7–9 μm). However, the surface of Pristine-NCA appears rough and there are many uneven dispersion of small particles. In contrast, we can find that P2-NCA obviously has a smoother surface morphology, which indicates the consumption of residual alkali on the surface and the formation of a coating layer. In addition, the EDS mapping was performed on P2-NCA. As shown in figures 3(e)–(h), the Ni, Co, Al and P
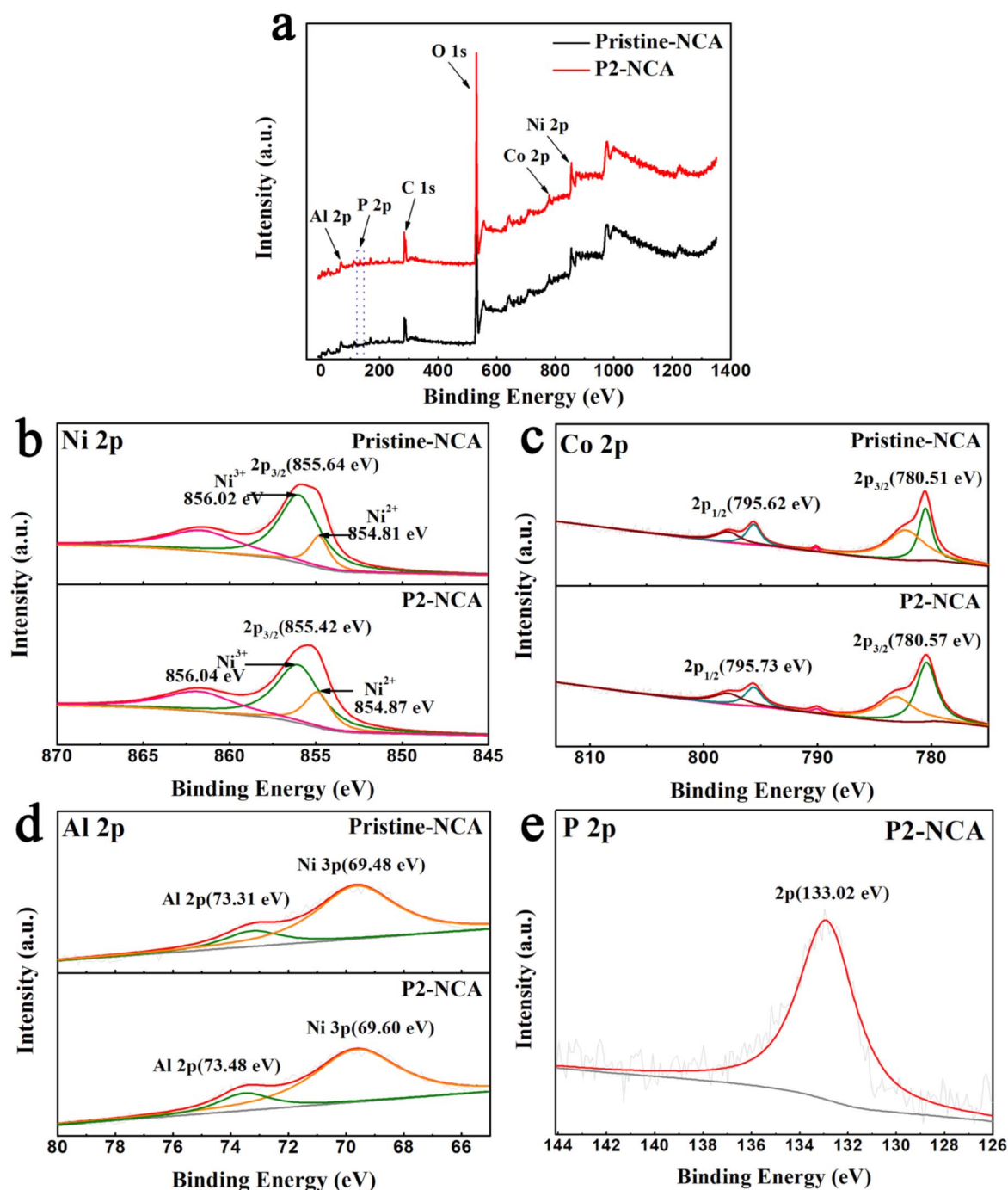
Figure 5. (a) Full XPS spectrum of Pristine-NCA and P2-NCA. XPS patterns of (b) Ni 2p, (c) Co 2p, (d) Al 2p for pristine-NCA and P2-NCA, and (e) P 2p for P2-NCA.

elements all show a uniform distribution, which means the successful introduction of phosphate [18].

The FETEM diagram of Pristine-NCA (figure 4(a)) shows a smooth surface. Furthermore, the high-resolution FETEM diagram of Pristine-NCA, obtained by further magnifying the box in figure 4(a), demonstrates a good crystallinity and a neatly arranged lattice structure. The interplanar spacing is about 0.47 nm, indicating the (003) crystal plane of NCA [19]. Additionally, it can be clearly found that there is an about 5 nm thick coating layer on the surface of P2-NCA (figure 4(c)) and the high-resolution FETEM diagram

(figure 4(d)) demonstrates that there is an obvious difference between site A and site B. Moreover, we measured the interlayer spacing of site A to be about 0.47 nm, which is consistent with the (003) crystal plane of NCA. Meanwhile, we also detected that the interlayer spacing of site B is about 0.264 nm, which corresponds to the (210) crystal plane of Li_3PO_4 [20]. This satisfactory result shows that LiH_2PO_4 successfully optimized the surface residual alkali and formed a Li_3PO_4 coating on the surface of NCA.

The XPS was used to detect the valence of transition metal elements in the samples and the P element in the coating
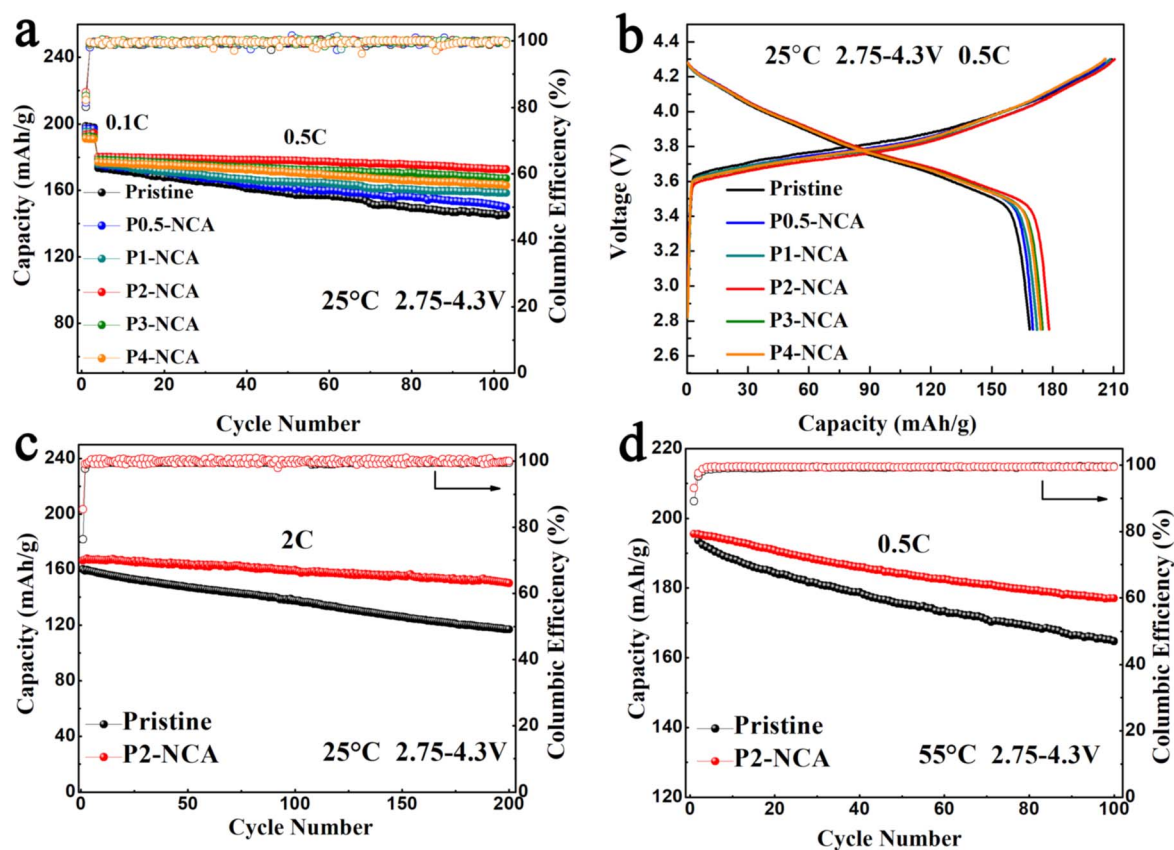
Figure 6. (a) Discharge capacity at 0.1 C, cycling behavior at 0.5 C and columbic efficiency in all cycles of Pristine-NCA, P0.5-NCA, P1-NCA, P2-NCA, P3-NCA and P4-NCA samples at 25 °C between 2.75 and 4.3 V. (b) Initial charge/discharge profiles of Pristine-NCA, P0.5-NCA, P1-NCA, P2-NCA, P3-NCA and P4-NCA samples at 0.5 C/25 °C (1 C = 200 mA g^{-1}). (c) Long-cycling behavior and columbic efficiency of Pristine-NCA and P2-NCA at 2 C/25 °C between 2.75 and 4.3 V. (d) Long-cycling behavior and columbic efficiency of Pristine-NCA and P2-NCA at 0.5 C/55 °C between 2.75 and 4.3 V.

layer. Figure 5(a) shows the full spectrum of Pristine-NCA and P2-NCA, which are very similar except that the characteristic peak of P 2p is detected in P2-NCA. As shown in figure 5(b), the Ni 2p spectra of Pristine-NCA and P2-NCA samples are divided into four peaks at 855.64 eV/855.42 eV (Ni^{3+}) and 854.81 eV/854.87 eV (Ni^{2+}), respectively, indicating that Ni^{2+} and Ni^{3+} are in a coexistent state in the samples [21, 22]. Additionally, as shown in figures 5(c) and (d), the peak positions of Co 2p and Al 2p show almost no changes before and after coating, which proves that the external presence of the coating layer does not affect the internal element valence states of Co and Al. Note that the characteristic peak of P 2p detected at 133.02 eV (figure 5(e)) is consistent with the P^{5+} in the report, which corresponds to the FETEM results [23]. Meanwhile, the single characteristic peak of the P element indicates the same chemical environment proving that the LiH$_2$PO$_4$ introduced in P2-NCA completely converted into Li$_3$PO$_4$, which is consistent with the pH results. The above results indicate that the P element has been successfully introduced into the surface of NCA and exists in the form of +5 valence.

Figure 6 shows the comprehensive evaluation of the electrochemical performance of the samples. Figure 6(a) shows the cycle performance of Pristine, P0.5-NCA, P1-NCA, P2-NCA, P3-NCA and P4-NCA at 25 °C/0.5 C (2.75–4.3 V), respectively. Since the weak polarization influence at the low rate of 0.1 C

towards the insertion and extraction of lithium ions from NCA cathode, the discharge capacities are 198.6 mAh g^{-1}, 197.2 mAh g^{-1}, 195.3 mAh g^{-1}, 193.5 mAh g^{-1}, 192.3 mAh g^{-1} and 191.2 mAh g^{-1}, respectively, showing a downward trend, which are attributed to the reduction of electrochemically active substances [24]. However, the initial columbic efficiency of all coated samples has been improved, indicating that the coating helps NCA acquire a more reversible phase transformation and a more stable electrode polarization [18]. Interestingly, owing to the fast ion conductor coating layer, the coated samples all show a higher discharge capacity than the Pristine at the high rate of 0.5 C. In addition, we found that its discharge capacity first increased and then decreased as the amount of phosphate added increases indicating that an overly thick coating layer is not conducive to its dynamic performance, which is consistent with the pH test results. Furthermore, we tested the long-cycle performance of all samples at 25 °C/0.5 C. The discharge capacity of Pristine dropped rapidly from 173.6 to 145.2 mAh g^{-1} after 100 cycles, showing the lowest capacity retention rate (83.6%), while that of P2-NCA dropped slowly from 180.2 to 172.6 mAh g^{-1} after 100 cycles, showing the highest capacity retention rate (95.8%). Meanwhile, the capacity retention rates of P0.5-NCA, P1-NCA, P3-NCA and P4-NCA are 85.3%, 90%, 94.2% and 92.1%, respectively, showing an improvement in cycle stability, which is also attributable to the effective protection of the NCA cathode
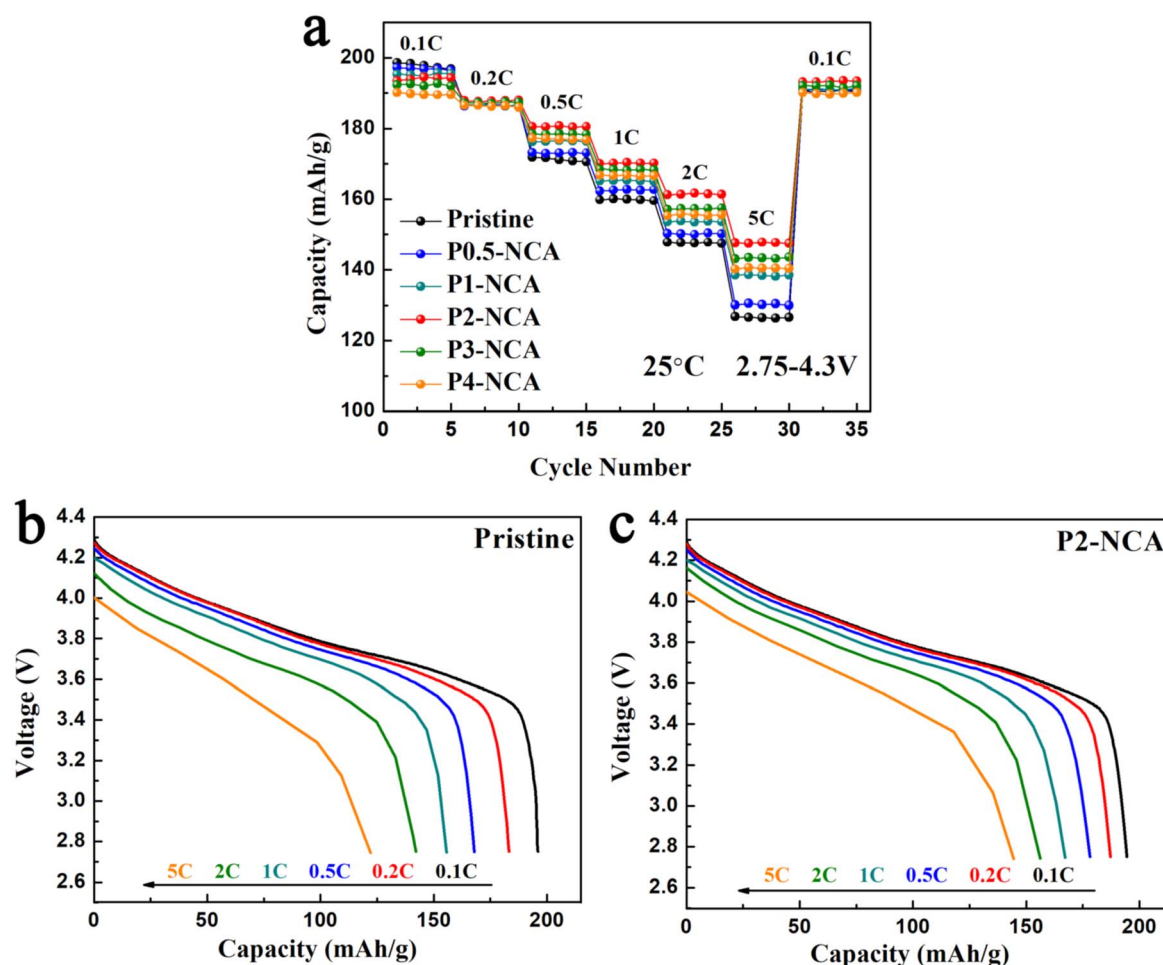
Figure 7. (a) Rate performance of all samples at 0.1 C, 0.2 C, 0.5 C, 1 C, 2 C, 5 C between 2.7 and 4.5 V and corresponding discharge profiles of (b) Pristine-NCA and (c) P2-NCA.

material by the coating layer [25]. Figure 6(b) is the initial charge/discharge profiles of all samples at 25 °C/0.5 C (2.75–4.3 V). P2-NCA provides the most discharge capacity and initial columbic efficiency (180.2 mAh g^{-1} and 84.7%) compared with Pristine-NCA (173.6 mAh g^{-1} and 78.7%). As shown in figure 6(c), to further verify the superiority of P2-NCA, we conducted a long cycle test at 25 °C/2 C. The results show that the capacity of P2-NCA decreases slowly from 166.4 to 150 mAh g^{-1} after 200 cycles, whose capacity retention rate is as high as 90.1%, whereas the capacity of Pristine-NCA decays rapidly from 160.1 to 117.1 mAh g^{-1} after 200 cycles and only provides a capacity retention rate of 73.1%. Furthermore, we conducted a high temperature cycle performance test at 55 °C/0.5 C (figure 6(d)), which show that the capacity retention rate of P2-NCA is as high as 90.8% compared to 81.9% of Pristine-NCA after 100 cycles. These results can be explained that the coating layer blocks the direct contact between the electrolyte and the material, thereby reducing the side reactions and the dissolution of transition metals and stabilizing the structure of the materials [26, 27].

Figure 7(a) shows the rate performance of all samples at 0.1 C, 0.2 C, 0.5 C, 1 C, 2 C, 5 C (2.75–4.3 V). As the rate increases, the capacity decays of all coated samples are less than that of Pristine-NCA, indicating the promotion effect of the coating layer

on the insertion and extraction of lithium ions. In addition, with the thickening of the coating layer, the discharge capacity showed a trend of first increasing and then decreasing, indicating that an excessively thick coating layer would hinder its dynamic performance. Figures 7(b) and (c) shows the corresponding discharge profiles of Pristine-NCA and P2-NCA. In contrast, the platform voltage of P2-NCA drops more gently, indicating superior electrochemical reversibility. Notably, P2-NCA exhibits a high discharge capacity of 147.8 mAh g^{-1} at a high rate of 5 C compared to Pristine-NCA (126.5 mAh g^{-1}), which benefits from the suitable fast ion conductor coating layer [28].

In order to characterize the degree of polarization of the material, Pristine-NCA and P2-NCA were tested by cyclic voltammetry (CV) at a scan rate of 0.1 mV s^{-1} (versus Li^+/Li) from 2.75 to 4.3 V. Generally, the potential difference between the oxidation peak and the reduction peak represents the degree of polarization of the material [29]. As shown in figures 8(a) and (b), the 1st and 2nd curves of P2-NCA show a smaller potential difference between the oxidation peak and the reduction peak compared with Pristine-NCA, which indicate a satisfactory degree of polarization of P2-NCA. Simultaneously, the coincidence of the 2nd and 3rd curves of P2-NCA indicates good electrochemical reversibility [30]. Furthermore, we have conducted the EIS of all samples after 1 cycle (figure 8(c)) and 100
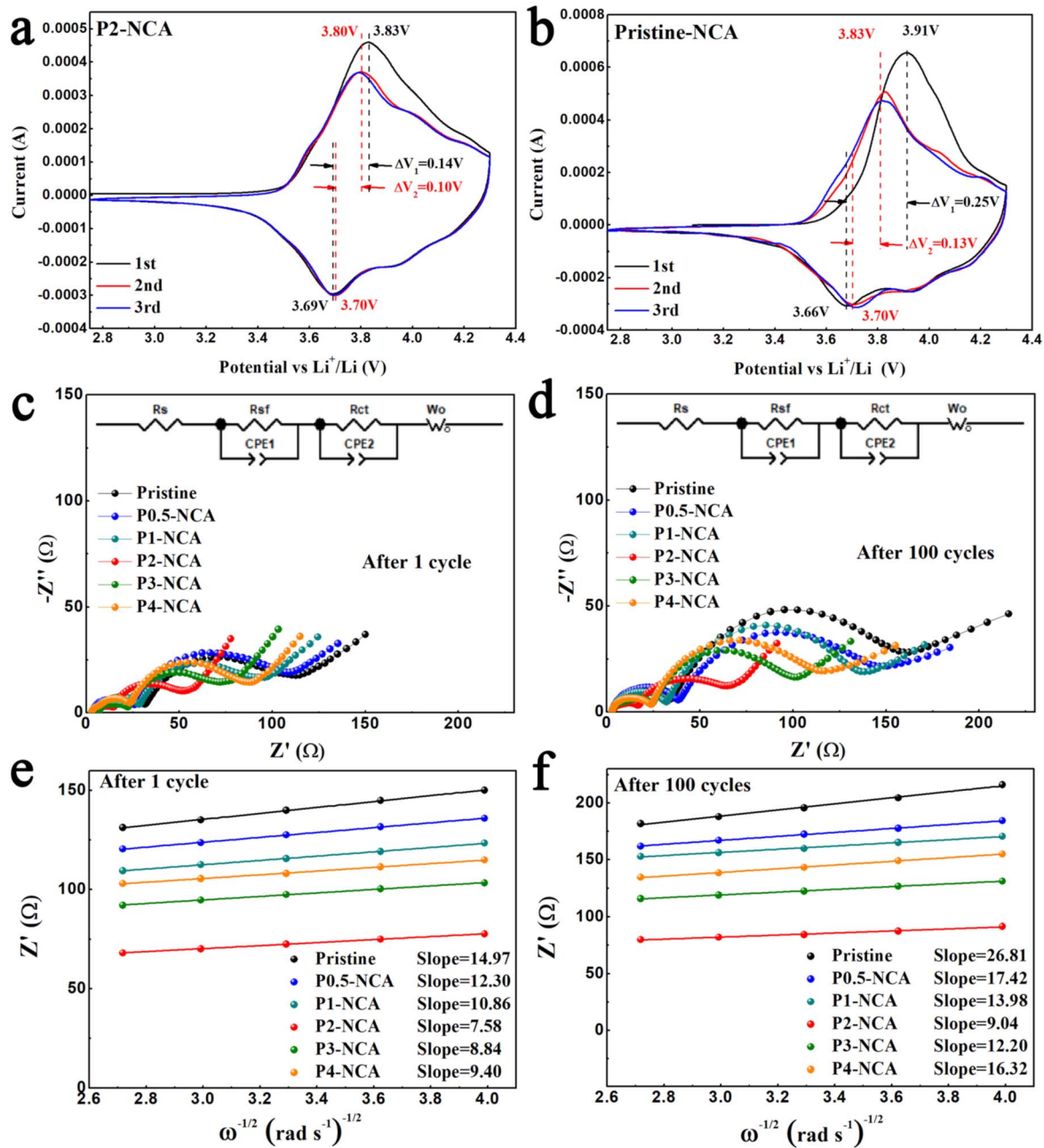
Figure 8. Cyclic voltammetry (CV) curves of (a) Pristine-NCA and (b) P2-NCA between 2.75 and 4.3 V at 0.1 mV s^{-1} (versus Li$^+$/Li). EIS for all samples (c) after 1 cycle and (d) after 100 cycles. Corresponding $Z'-\omega^{-0.5}$ fitting curves for all samples (e) after 1 cycle and (f) after 100 cycles.

cycles (figure 8(d)). The Nyquist curves, obtained by fitting in the equivalent circuit, are composed of a semicircle in the high-frequency region, a semicircle in the intermediate frequency region, and a straight line in the low-frequency region, representing membrane impedance (R_{sf}), charge transfer impedance (R_{ct}), and Warburg impedance (W_o), respectively [31, 32]. According to table 2, with the increase of the coating amount, both the R_{sf} value and the R_{ct} value show a trend of first decreasing and then increasing, which is consistent with the rate performance results. The R_{sf} value of P2-NCA changes less than Pristine-NCA after 100 cycles, which substantiates that it forms a more stable SEI film and inhibits the thickening of the SEI film

[33]. In addition, we canalso find that the initial R_{ct} value of P2-NCA is significantly smaller than that of Pristine-NCA, implying that the fast ion conductor contributes to the ion charge transfer during the insertion and de-embedding of Li$^+$ [34]. Notably, the R_{ct} value of Pristine-NCA increases rapidly after cycling, which is considered to be irreversible microstructure degradation [35]. In contrast, the R_{ct} value of P2-NCA is small and grows slowly, indicating that the coating layer can effectively protect the surface of NCA and reduce its structural degradation [36]. More importantly, the corresponding graphs (figures 8(e) and (f)) and data (table 3) are obtained by fitting the data in the low-frequency region [37]. The slope (σ) of the straight line in the figure is
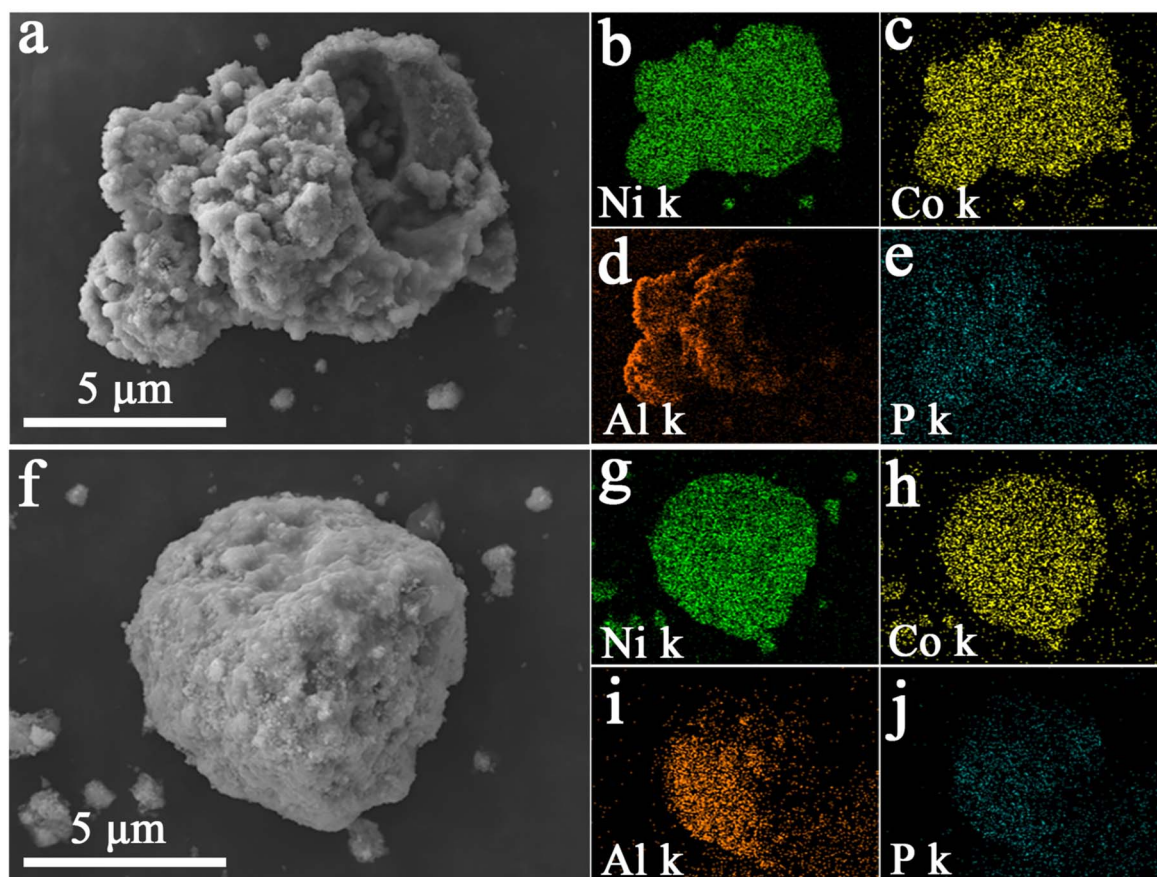
Figure 9. SEM images of (a) Pristine-NCA and its corresponding EDS mapping of (b) Ni, (c) Co, (d) Al and (e) P after 100 cycles; SEM images of (f) P2-NCA and its corresponding EDS mapping of (g) Ni, (h) Co, (i) Al and (j) P after 100 cycles.

Table 2. EIS parameters of all samples.

Electrodes (1 cycle)	R_{sf} (Ω)	R_{ct} (Ω)
Pristine-NCA	23.78	62.58
P0.5-NCA	20.44	60.68
P1-NCA	19.03	51.09
P2-NCA	9.57	26.31
P3-NCA	13.52	30.67
P4-NCA	22.99	48.94
Electrodes (100 cycles)	R_{sf} (Ω)	R_{ct} (Ω)
Pristine-NCA	30.73	115.2
P0.5-NCA	33.52	101.4
P1-NCA	28.22	96.45
P2-NCA	13.07	44.33
P3-NCA	21.98	62.68
P4-NCA	22.06	78.50

Table 3. σ data and D_{Li+} of all samples after 1 cycle and 100 cycles.

Electrodes (1 cycle)	σ	Standard error	D_{Li+} (cm^2 s^{-1})
Pristine-NCA	14.97	0.218	1.96×10^{-12}
P0.5-NCA	12.30	0.141	1.71×10^{-12}
P1-NCA	10.86	0.137	2.20×10^{-12}
P2-NCA	7.58	0.042	4.52×10^{-12}
P3-NCA	8.84	0.169	3.32×10^{-12}
P4-NCA	9.40	0.156	2.94×10^{-12}
Electrodes (100 cycles)	σ	Standard error	D_{Li+} (cm^2 s^{-1})
Pristine-NCA	26.81	0.991	3.62×10^{-13}
P0.5-NCA	17.42	0.298	8.57×10^{-13}
P1-NCA	13.98	0.503	1.33×10^{-12}
P2-NCA	9.04	0.477	3.18×10^{-12}
P3-NCA	12.20	0.131	1.75×10^{-12}
P4-NCA	16.32	0.298	9.76×10^{-13}

inversely proportional to the Li$^+$ diffusion coefficient (D_{Li+}), which can be calculated according to formula 1 [38]. As shown in table 3, the smaller standard error value proves the high reliability of the results. The D_{Li+} of Pristine-NCA is 1.96×10^{-12} cm^2 s^{-1} and 3.62×10^{-13} cm^2 s^{-1}, while P2-NCA is 4.52×10^{-12} cm^2 s^{-1} and 3.18×10^{-12} cm^2 s^{-1} after 1 cycle and 100 cycles, respectively. The smaller σ value of P2-NCA corresponds to the larger Li$^+$ diffusion coefficient (D_{Li+}), indicating that the fast ion

conductor coating greatly enhances the lithium-ion transport capacity on the surface of NCA

$$D_{Li+} = \frac{R^2 T^2}{2A^2 n^4 F^4 C^2 \sigma^2}.$$

Formula 1. Li$^+$ diffusion coefficient calculation formula, where R is the gas constant, T is the absolute temperature constant, A is the electroactive area of the cathode material, n is the number of

electrons in the electrochemical process, F is the Faraday constant, C is the Li$^+$ concentration in the cathode material, σ is the slope of $Z'-\omega^{-0.5}$ fitting curves.

The SEM measurements were also carried out to investigate the surface morphology of Pristine-NCA and P2-NCA samples after 100 cycles. Incontrovertibly, the surface structure of the secondary particles of Pristine-NCA is severely degraded and collapsed (figure 9(a)), which is ascribed to the continuous erosion of the secondary particles by the Lewis acid produced by the hydrolysis of LiPF$_6$ [8]. The distribution of the Ni, Co and Al elements show almost no changes after cycles (figures 9(b)–(d)). Particularly, the EDS mapping image of Pristine-NCA after 100 cycles exhibits that the P element (figure 9(e)) is detected on the surface and inside, which further substantiates the corrosion effect of the electrolyte on the secondary particles. In contrast, the SEM (figure 9(f)) and EDS mapping (figures 9(g)–(j)) analyses conclude that P2-NCA can maintain its spherical morphology and the distribution of Ni, Co, Al and P elements also are still in nature after 100 cycles. Therefore, the phosphate coating layer outstandingly ameliorates the surface stability of the P2-NCA cathode material, which is beneficial to inhibit side reactions.

4. Conclusion

In summary, we successfully developed a satisfactory electrochemical performance via the phosphate coating. On the one hand, the phosphate coating layer structure can avoid direct contact between NCA and electrolyte, thereby reducing side reactions during charging and discharging and improving the cycle stability of NCA cathode materials. On the other hand, the introduced LiH$_2$PO$_4$ can react with the residual alkali on the surface to form a fast ion conductor coating to improve the dynamic performance of the NCA cathode material. As expected, the phosphate coating effectively optimizes the residual alkali on the surface, reduces side reactions and generate fast ion conductor coating layer, thereby improving the cycling stability and rate performance of NCA. Therefore, this work not only provides us with an attractive coating material for improving the electrochemical performance of NCA but also opens up a new path to explore phosphates for optimizing the residual alkali on the surface of NCA.

Data availability statement

All data that support the findings of this study are included within the article (and any supplementary files).

ORCID iDs

Wendong Cheng ⬤ https://orcid.org/0000-0003-3285-9031

References

[1] Liu W, Oh P, Liu X, Lee M J, Cho W, Chae S, Kim Y and Cho J 2015 Nickel-rich layered lithium transition-metal oxide for high-energy lithium-ion batteries *Angew. Chem., Int. Ed.* **54** 4440–57

[2] Kim J, Lee H, Cha H, Yoon M, Park M and Cho J 2018 Nickel-rich cathodes: prospect and reality of Ni-rich cathode for commercialization *Adv. Energy Mater.* **8** 1870023

[3] Scrosati B and Garche J 2010 Lithium batteries: status, prospects and future *J. Power Sources* **195** 2419–30

[4] Zhang Z, Zhou P, Meng H, Chen C, Cheng F, Tao Z and Chen J 2017 Amorphous Zr(OH)$_4$ coated LiNi$_{0.915}$Co$_{0.075}$Al$_{0.01}$O$_2$ cathode material with enhanced electrochemical performance for lithium ion batteries *J. Energy Chem.* **3** 481–7

[5] Chen C, Liu J and Stoll M E 2004 Aluminum-doped lithium nickel cobalt oxide electrodes for high-power lithium-ion batteries *J. Power Sources* **128** 278–85

[6] Xia Y, Zheng J, Wang C and Gu M 2018 Designing principle for Ni-rich cathode materials with high energy density for practical applications *Nano Energy* **49** 434–52

[7] Fu J, Mu D, Wu B, Bi J, Cui H, Yang H, Wu H and Wu F 2018 Electrochemical properties of the LiNi$_{0.6}$Co$_{0.2}$Mn$_{0.2}$O$_2$ cathode material modified by lithium tungstate under high voltage *ACS Appl. Mater. Inter.* **10** 19704–11

[8] Zhang S 2020 Problems and their origins of Ni-rich layered oxide cathode materials *Energy Storage Mater.* **24** 247–54

[9] Zheng J, Yang Z, He Z, Tong H, Yu W and Zhang J 2018 *In situ* formed LiNi$_{0.8}$Co$_{0.15}$Al$_{0.05}$O$_2$@Li$_4$SiO$_4$ composite cathode material with high-ratecapability and long cycling stability for lithium-ion batteries *Nanomater. Energy* **53** 613–21

[10] Hu S, Cheng G, Cheng M, Hwang B J and Santhanam R 2009 Cycle life improvement of ZrO$_2$-coated spherical LiNi$_{1/3}$Co$_{1/3}$Mn$_{1/3}$O$_2$ cathode material for lithium ion batteries *J. Power Sources* **188** 564–9

[11] Jang S, Kang S, Amine K, Bae Y and Sun Y 2005 Synthesis and improved electrochemical performance of Al(OH)$_3$-coated Li[Ni$_{1/3}$Mn$_{1/3}$Co$_{1/3}$]O$_2$ cathode materials at elevated temperature *Electrochim. Acta* **50** 4168–73

[12] Zhou P, Zhang Z, Meng H, Lu Y, Cao J, Cheng F, Tao Z and Chen J 2016 SiO$_2$-coated LiNi$_{0.915}$Co$_{0.075}$Al$_{0.01}$O$_2$ cathode material for rechargeable Li-ion batteries *Nanoscale* **8** 19263–9

[13] Liu C, Cao G, Wu Z, Hu J, Wang H and Shao G 2019 Surficial structure retention mechanism for LiNi$_{0.8}$Co$_{0.15}$Al$_{0.05}$O$_2$ in a full gradient cathode *ACS Appl. Mater. Inter.* **11** 31991–6

[14] Qi R, Shi J, Zhang X, Zeng X, Yin Y, Xu J, Chen L, Fu W, Guo Y and Wan L 2017 Improving the stability of LiNi$_{0.80}$Co$_{0.15}$Al$_{0.05}$O$_2$ by AlPO$_4$ nanocoating for lithium-ion batteries *Sci. China Chem.* **60** 1230–5

[15] Yi T, Li Y, Li X, Pan J, Zhang Q and Zhu Y 2017 Enhanced electrochemical property of FePO4-coated LiNi$_{0.5}$Mn$_{1.5}$O$_4$ as cathode materials for Li-ion battery *Sci. Bull.* **62** 1004–10

[16] Wu Z, Ji S, Liu T, Duan Y, Xiao S, Lin Y, Xu K and Pan F 2016 Aligned Li + tunnels in core–shell Li(NixMnyCoz)O$_2$@LiFePO$_4$ enhances its high voltage cycling stability as Li-ion battery cathode *Nano Lett.* **16** 6357–63

[17] Zang D, Zhu R, Zhang W, Wu J, Yu X and Zhang Y 2014 Stearic acid modified aluminum surfaces with controlled wetting properties and corrosion resistance *Corros. Sci.* **83** 86–93

[18] Zhao S, Shao L, Li X, Yang L, Wei B, Yang Y, Zhao H, Yin D, Ma W and Wang Z 2020 Acid-corrosion-formed amorphous phosphate surfaces improve electrochemical stability of LiNi$_{0.80}$Co$_{0.15}$Al$_{0.05}$O$_2$ cathodes *Corros. Sci.* **168** 108553

[19] Zheng J, Yang Z, Dai A, Tang L, Wei H, Li Y, He Z and Lu J 2019 Boosting cell performance of LiNi$_{0.8}$Co$_{0.15}$Al$_{0.05}$O$_2$ via surface structure design *Small* **15** 1904854

[20] Ran Q *et al* 2019 Dual functions of gradient phosphate polyanion doping on improving the electrochemical performance of Ni-rich LiNi$_{0.6}$Co$_{0.2}$Mn$_{0.2}$O$_2$ cathode at high cut-off voltage and high temperature *Electrochim. Acta* **299** 971–8

[21] Wu F, Tian J, Su Y, Wang J, Zhang C, Bao L, He T, Li J and Chen S 2015 Effect of Ni^{2+} content on lithium/nickel disorder for Ni-rich cathode materials *ACS Appl. Mater. Inter.* **7** 7702–8

[22] Zhang X, Belharouak I, Li L, Lei Y, Elam J, Nie A, Chen X, Yassar R and Axelbaum R 2013 Structural and electrochemical study of Al$_2$O$_3$ and TiO$_2$ coated Li$_{1.2}$Ni$_{0.13}$Mn$_{0.54}$Co$_{0.13}$O$_2$ cathode material using *ALD Adv. Energy Mater.* **3** 1299–307

[23] Bian X, Fu Q, Bie X, Yang P, Qiu H, Pang Q, Chen G, Du F and Wei Y 2015 Improved electrochemical performance and thermal stability of Li-excess Li$_{1.18}$Co$_{0.15}$Ni$_{0.15}$Mn$_{0.52}$O$_2$ cathode material by Li$_3$PO$_4$ surface coating *Electrochim. Acta* **174** 875–84

[24] Xia S, Huang W, Shen X, Liu J, Cheng F, Liu J, Yang X and Guo H 2020 Rearrangement on surface structures by boride to enhanced cycle stability for LiNi$_{0.80}$Co$_{0.15}$Al$_{0.05}$O$_2$ cathode in lithium ion batteries *J. Energy Chem.* **45** 110–8

[25] Chen S, He T, Su Y, Lu Y, Bao L, Chen L, Zhang Q, Wang J, Chen R and Wu F 2017 Ni-rich LiNi$_{0.8}$Co$_{0.1}$Mn$_{0.1}$O$_2$ oxide coated by dual-conductive layers as high performance cathode material for lithium-ion batteries *ACS Appl. Mater. Interfaces* **9** 29732–43

[26] Watanabe S, Kinoshita M, Hosokawa T, Morigaki K and Nakura K 2014 Capacity fade of LiAl$_y$Ni$_{1−x−y}$Co$_x$O$_2$ cathode for lithium-ion batteries during accelerated calendar and cycle life tests (surface analysis of LiAlyNi$_{1−x−y}$Co$_x$O$_2$ cathode after cycle tests in restricted depth of discharge ranges) *J. Power Sources* **258** 210–7

[27] Mu K, Cao Y, Hu G, Du K, Yang H, Gan Z and Peng Z 2018 Enhanced electrochemical performance of Li-rich cathode Li$_{1.2}$Ni$_{0.2}$Mn$_{0.6}$O$_2$ by surface modification with WO$_3$ for lithium ion batteries *Electrochim. Acta* **273** 88–97

[28] Liu W *et al* 2018 Significantly improving cycling performance of cathodes in lithium ion batteries: the effect of Al$_2$O$_3$ and

LiAlO$_2$ coatings on LiNi$_{0.6}$Co$_{0.2}$Mn$_{0.2}$O$_2$ *Nano Energy* **44** 111–20

[29] Jamil S, Wang G, Yang L, Xie X, Cao S, Liu H, Chang B and Wang X 2020 Suppressing H2–H3 phase transition in high Ni–low Co layered oxide cathode material by dual modification *J. Mater. Chem.* A **8** 21306

[30] Feng D, Liu Q, Hu T, Chen Y and Zeng T 2021 Boosting cyclability performance of the LiNi$_{0.8}$Co$_{0.15}$Al$_{0.05}$O$_2$ cathode by a polyacrylonitrile-induced conductive carbon surface coating *Ceram. Int.* **47** 12706–15

[31] Zheng J M, Kan W H and Manthiram A 2015 Role of Mn content on the electrochemical properties of Nickel-rich layered LiNi$_{0.8−x}$Co$_{0.1}$Mn$_{0.1+x}$O$_2$ (0.0 ⩽ x ⩽0.08) cathodes for lithium-ion batteries *ACS Appl. Mater. Interfaces* **7** 6926–34

[32] Zhang C, Wan J, Li Y, Zheng S, Zhou K, Wang D, Wang D, Hong C, Gong Z and Yang Y 2020 Restraining the polarization increase of Ni-rich and low-Co cathodes upon cycling by Al-doping *J. Mater. Chem.* A **8** 6893

[33] Chen T, Li X, Wang H, Yan X, Wang L, Deng B, Ge W and Qu M 2018 The effect of gradient boracic polyanion-doping on structure, morphology, and cycling performance of Ni-rich LiNi$_{0.8}$Co$_{0.15}$Al$_{0.05}$O$_2$ cathode material *J. Power Sources* **374** 1–11

[34] Zheng J, Engelhard M H, Mei D, Jiao S, Polzin B J, Zhang J and Xu W 2017 Electrolyte additive enabled fast charging and stable cycling lithium metal batteries *Nat. Energy* **2** 17012

[35] Xu C, Xiang W, Wu Z, Xu Y, Li Y, Chen M, Guo X, Lv G, Zhang J and Zhong B 2018 Constructing a protective pillaring layer by incorporating gradient Mn^{4+} to stabilize the surface/interfacial structure of LiNi$_{0.815}$Co$_{0.15}$Al$_{0.035}$O$_2$ cathode *ACS Appl. Mater. Interfaces* **10** 27821–30

[36] Wang L *et al* 2018 TiS$_2$ as a high performance potassium ion battery cathode in ether-based electrolyte *Energy Storage Mater.* **12** 216–22

[37] Ran Q *et al* 2018 Enhanced electrochemical performance of dual-conductive layers coated Ni-rich LiNi$_{0.6}$Co$_{0.2}$Mn$_{0.2}$O$_2$ cathode for Li-ion batteries at high cut-off voltage *Electrochim. Acta* **289** 82–93

[38] Zhang L, Wang J, Yang X, Liang G, Li T, Yu P and Ma D 2018 Enhanced electrochemical performance of fast ionic conductor LiTi$_2$(PO$_4$)3-coated LiNi$_{1/3}$Co$_{1/3}$Mn$_{1/3}$O$_2$ cathode material *ACS Appl. Mater. Interfaces* **10** 11663–70